Supplementary Information

Dynamic Evolution of Higher Alcohols from CO_2 on Fe_3O_4-Fe_5C_2-Cu Catalytic Interfaces with amorphous Ti Layout

Teng Li [1, 2, 3*], Lijun Zhang [4], Zhenkun Liu [2], Jiaming Liang [2], Hao Chen [2], Linlin Zhao [2], Shunnosuke Fujii [2], Peng Qin [2], Qiang Liu [5], Tao Li [5], Tao Xing [5], Jiancai Sui [5], Yongqiang Gu [5], Minghui Tan [1], Mingbo Wu [1*], Zhiliang Jin [3*], Noritatsu Tsubaki [2*]

[1] College of Chemical Engineering, Qingdao University of Science & Technology, Qingdao 266100, China

[2] Department of Applied Chemistry, Graduate School of Engineering, University of Toyama, Gofuku 3190, Toyama 930-8555, Japan

[3] School of Chemistry and Chemical Engineering, North Minzu University, Yinchuan 750021, P. R. China

[4] School of Chemistry & Chemical Engineering, Anhui University of Technology, Ma'anshan, Anhui, 243002, China

[5] Shandong Energy Group Co., Ltd, Jinan, Shandong 250101, China

*Corresponding author. E-mail: tengli@eng.u-toyama.ac.jp (Teng Li)
wumb@upc.edu.cn (Mingbo Wu)
zl-jin@nun.edu.cn (Zhiliang Jin)
tsubaki@eng.u-toyama.ac.jp (Noritatsu Tsubaki)

Supplementary Figures and Tables

Supplementary Figure 1. The catalytic performance of CO_2 hydrogenation for different catalysts. a CO_2 hydrogenation performance of different Fe-based catalysts. **b** Percentage of higher alcohols in the alcohol and the STY of higher alcohols for different iron-based catalysts. Reaction conditions: 5.0 MPa, 320 °C, feed gas (Ar 5 vol%, CO_2 27 vol%, H_2 68 vol%), GHSV = 4800 mL g_{cat}^{-1} h^{-1}.

Supplementary Figure 2. The catalytic performance of CO_2 hydrogenation under different pressures. a CO_2 hydrogenation performance of 1%Na-$FeTiO_x$ under different pressure. **b** Percentage of higher alcohols in the alcohol and the STY of higher alcohols for 1%Na-$FeTiO_x$ under different pressure. Reaction conditions: 320 °C, feed gas (Ar 5 vol%, CO_2 27 vol%, H_2 68 vol%), GHSV = 4800 mL g_{cat}^{-1} h^{-1}.

Supplementary Figure 3. The catalytic performance of CO_2 hydrogenation under different Na content. a CO_2 hydrogenation performance of $FeTiO_x$ under different Na contents. **b** Percentage of higher alcohols in the alcohol and the STY of higher alcohols for $FeTiO_x$ under different Na contents. Reaction conditions: 5.0 MPa, 320 °C, feed gas (Ar 5 vol%, CO_2 27 vol%, H_2 68 vol%), GHSV = 4800 mL g_{cat}^{-1} h^{-1}.

Supplementary Figure 4. The Catalytic performance of CO_2 hydrogenation under different feed gas. a CO_2 hydrogenation performance of 1%Na-$FeTiO_x$ under different feed gas (H_2/CO_2=2.0: Ar 4 vol%, CO_2 32 vol%, H_2 64 vol%. H_2/CO_2=2.5: Ar 5 vol%, CO_2 27 vol%, H_2 68 vol%. H_2/CO_2=3.0: Ar 4 vol%, CO_2 24 vol%, H_2 72 vol%.). **b** Percentage of higher alcohols in the alcohol and the STY of higher alcohols for $FeTiO_x$ under different feed gas (H_2/CO_2=2.0: Ar 4 vol%, CO_2 32 vol%, H_2 64 vol%. H_2/CO_2=2.5: Ar 5 vol%, CO_2 27 vol%, H_2 68 vol%. H_2/CO_2=3.0: Ar 4 vol%, CO_2 24 vol%, H_2 72 vol%.). Reaction conditions: 5.0 MPa, 320 °C, GHSV = 4800 mL g_{cat}^{-1} h^{-1}.

Supplementary Figure 5. The results of CO_2-TPD for different catalysts. CO_2-TPD spectra of 1%Na-Fe_2O_3, 1%Na-$FeTiO_x$ and 1%Na-$Cu_{0.10}FeTiO_x$.

Supplementary Figure 6. The results of CO-TPD for different catalysts. CO-TPD spectra of spent 1%Na-Fe_2O_3,1%Na-$FeTiO_x$, 1%Na-TiO_2-Fe_2O_3 and 1%Na-$Cu_{0.10}FeTiO_x$.

Supplementary Figure 7. The results of H_2-TPD for different catalysts. H_2-TPD spectra of 1%Na-$FeTiO_x$ and 1%Na-$Cu_{0.10}FeTiO_x$.

Supplementary Figure 8. The catalytic performance of CO_2 hydrogenation under different temperatures. a CO_2 hydrogenation performance of 1% Na-$Cu_{0.10}FeTiO_x$ under different temperatures. Reaction conditions: 5.0 MPa, CO_2: H_2 =1:2.5, GHSV = 4800 mL $gcat^{-1}$ h^{-1}. **b** Product distribution excluding CO of CO_2 hydrogenation at 340 °C for 1% Na-$Cu_{0.10}FeTiO_x$. Reaction conditions: 5.0 MPa, 340 °C, feed gas (Ar 5 vol%, CO_2 27 vol%, H_2 68 vol%), GHSV = 8000 mL g_{cat}^{-1} h^{-1}.

Supplementary Figure 9. The catalytic performance of CO_2 hydrogenation under different temperatures. a Alcohol distribution of 1% Na-$Cu_{0.10}FeTiO_x$ under different temperatures. Reaction conditions: 5.0 MPa, CO_2: H_2 =1:2.5, GHSV = 4800 mL $gcat^{-1}$ h^{-1}. **b** Percentage of alcohols excluding CO for 1% Na-$Cu_{0.10}FeTiO_x$ at 340 °C. Reaction conditions: 5.0 MPa, 340 °C, feed gas (Ar 5 vol%, CO_2 27 vol%, H_2 68 vol%), GHSV = 8000 mL g_{cat}^{-1} h^{-1}.

Supplementary Figure 10. The catalytic performance of CO_2 hydrogenation under different temperatures. a Percentage of higher alcohols in the alcohol and the STY of higher alcohols for different iron-based catalysts. Reaction conditions: 5.0 MPa, CO_2: H_2 =1:2.5, GHSV = 4800 mL $gcat^{-1}$ h^{-1}. **b** Percentage of different alcohols in the alcohol phase of 1% Na-$Cu_{0.10}FeTiO_x$ at 340 °C. Reaction conditions: 5.0 MPa, 340 °C, feed gas (Ar 5 vol%, CO_2 27 vol%, H_2 68 vol%), GHSV = 8000 mL g_{cat}^{-1} h^{-1}.

Supplementary Figure 11. The catalytic stability of CO_2 hydrogenation for 1%Na-$Cu_{0.10}FeTiO_x$. Catalytic stability of 1%Na-$Cu_{0.10}FeTiO_x$ catalyst for CO_2 hydrogenation. Reaction conditions: 5.0 MPa, 340 °C, feed gas (Ar 5 vol%, CO_2 27 vol%, H_2 68 vol%), GHSV = 4800 mL g_{cat}^{-1} h^{-1}.

Supplementary Figure 12. The phase structure of 1% Na-TiO_2-Fe_2O_3 and 1%Na-$FeTiO_X$. XRD patterns of 1%Na-TiO_2-Fe_2O_3 (a) and 1%Na-$FeTiO_x$ (b).

Supplementary Figure 13. The phase structure of 1%Na-$Cu_{0.10}FeTiO_X$. XRD patterns of 1%Na-$Cu_{0.10}FeTiO_x$.

Supplementary Figure 14. The morphological characteristics and element distribution of 1%Na-$FeTiO_x$. SEM and SEM-Mapping of 1%Na-$FeTiO_x$.

Supplementary Figure 15. The morphological characteristics and element distribution of 1%Na-$Cu_{0.10}FeTiO_x$. SEM and SEM-Mapping of 1%Na-$Cu_{0.10}FeTiO_x$.

Supplementary Figure 16. The microscopic morphological characteristics and element distribution of $FeTiO_x$ and $Cu_{0.10}FeTiO_x$. TEM and TEM-Mapping of $FeTiO_x$ (a) and $Cu_{0.10}FeTiO_x$ (b).

Supplementary Figure 17. The results of BET for 1%Na-$FeTiO_x$ and 1%Na-$Cu_{0.10}FeTiO_x$. a N_2 adsorption-desorption isotherms of 1%Na-$FeTiO_x$ and 1%Na-$Cu_{0.10}FeTiO_x$. **b** Pore size distributions of 1%Na-$FeTiO_x$ and 1%Na-$Cu_{0.10}FeTiO_x$.

Supplementary Figure 18. The results of BET for different catalysts. a N_2 adsorption-desorption isotherms of 1%Na-$FeTiO_x$ with different Cu doping amounts. **b** Pore size distributions of 1%Na-$FeTiO_x$ with different Cu doping amounts.

Supplementary Figure 19. The results of Fe 2*p* and Ti 2*p* XPS fine spectra for fresh catalysts. a Fe 2*p* XPS fine spectra of 1%Na-$FeTiO_x$ and 1%Na-$Cu_{0.10}FeTiO_x$. **b** Ti 2*p* XPS fine spectra of 1%Na-$FeTiO_x$ and 1%Na-$Cu_{0.10}FeTiO_x$.

Supplementary Figure 20. The results of Cu 2*p* and Cu LMM XPS fine spectra for fresh catalysts. a Cu 2*p* XPS fine spectra of 1%Na-$Cu_{0.10}FeTiO_x$. **b** Cu LMM XPS fine spectra of 1%Na-$Cu_{0.10}FeTiO_x$.

Supplementary Figure 21. The results of Cu 2*p* XPS fine spectra for spent 1%Na-$Cu_{0.10}FeTiO_x$. Cu 2*p* XPS fine spectra of spent 1%Na-$Cu_{0.10}FeTiO_x$.

Supplementary Figure 22. The phase structure of spent 1%Na-$FeTiO_x$. XRD patterns of spent 1%Na-$FeTiO_x$.

Supplementary Table 1 Catalytic performances of different iron-based catalysts.

Supplementary Table 2 Catalytic performances of different iron-based catalysts.

Supplementary Table 3 Catalytic performances of 1%Na-$Cu_{0.10}FeTiO_x$ under different space velocities.

Supplementary Table 4 Catalytic performances of 1%Na-$Cu_{0.10}FeTiO_x$ under different temperatures.

Supplementary Table 5. Catalytic results of various Fe-based catalysts for CO_2 hydrogenation to higher alcohols.

Supplementary Table 6 The Mean pore size, Pore volume and S_{BET} of different catalysts.

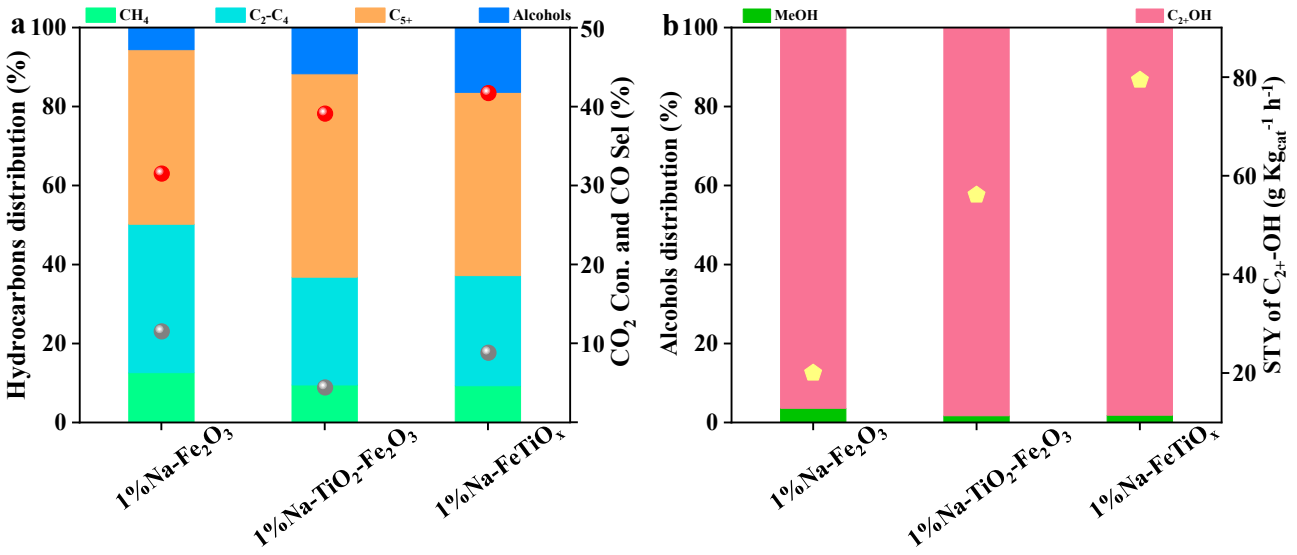

Supplementary Figure 1. The catalytic performance of CO_2 hydrogenation for different catalysts. a CO_2 hydrogenation performance of different Fe-based catalysts. **b** Percentage of higher alcohols in the alcohol and the STY of higher alcohols for different iron-based catalysts. Reaction conditions: 5.0 MPa, 320 °C, feed gas (Ar 5 vol%, CO_2 27 vol%, H_2 68 vol%), GHSV = 4800 mL g_{cat}^{-1} h^{-1}.

Note:

To further investigate the effect of amorphous Ti on the catalytic conversion of CO_2 to higher alcohols, the catalytic activity of both the amorphous iron-based catalyst and the pure iron catalyst was further investigated. As shown in Supplementary Figure 1 and Supplementary Table 1, with the introduction of metallic Ti, CO_2 conversion was further improved (from 31.5% to 41.7%), and CO selectivity was suppressed to varying degrees (from 11.5% to 4.4%). At the same time, the selectivity for higher alcohols was further significantly enhanced (from 5.4% to 16.1%), indicating that the introduction of metallic Ti effectively promotes CO_2 conversion and the directed formation of higher alcohols. Furthermore, a comparison of the catalytic results for crystalline and amorphous Ti revealed that the introduction of amorphous Ti metal is more effective in promoting the synthesis of higher alcohols, which fully demonstrates that the $FeTiO_x$ system featuring an amorphous Ti coordination environment possesses an intrinsic propensity for higher alcohols formation.

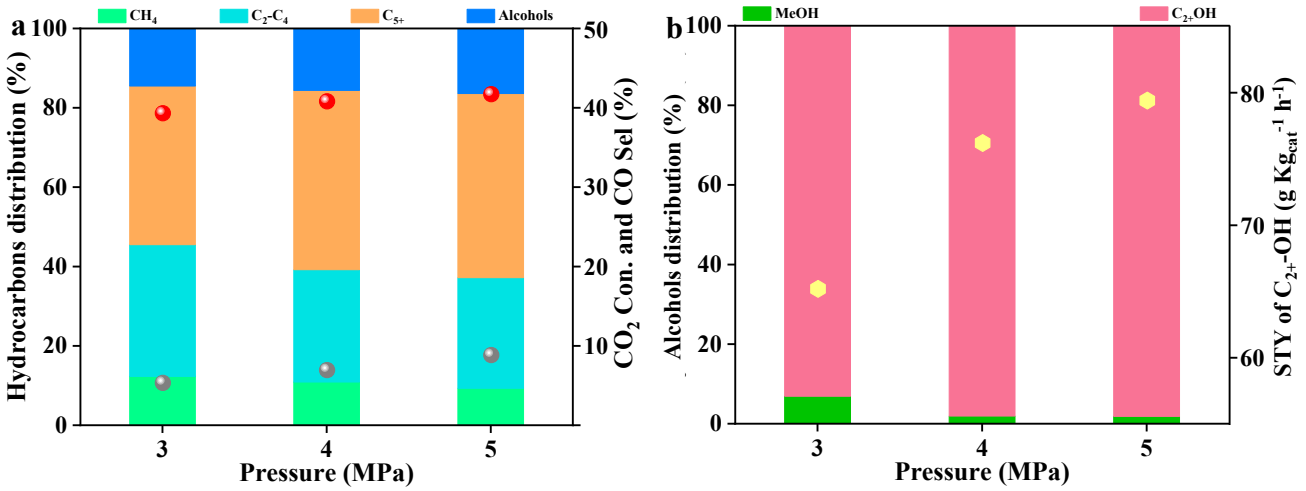

Supplementary Figure 2. The catalytic performance of CO_2 hydrogenation under different pressures. a CO_2 hydrogenation performance of 1%Na-$FeTiO_x$ under different pressure. **b** Percentage of higher alcohols in the alcohol and the STY of higher alcohols for 1%Na-$FeTiO_x$ under different pressure. Reaction conditions: 320 °C, feed gas (Ar 5 vol%, CO_2 27 vol%, H_2 68 vol%), GHSV = 4800 mL g_{cat}^{-1} h^{-1}.

Note:

Regulating the pressure of the reaction system is beneficial for optimizing the equilibrium reaction rate and product selectivity. Based on this, the effects of different pressures were further investigated. The results indicate that increasing pressure improves the conversion of CO_2, suppresses the formation of CH_4, and enhances the directed synthesis of higher alcohols to some extent (Supplementary Figure 2 And Supplementary Table 2). The results show that 1% Na-$FeTiO_x$ exhibits better CO_2 conversion and higher alcohols selectivity under conditions of 5.0 MPa.

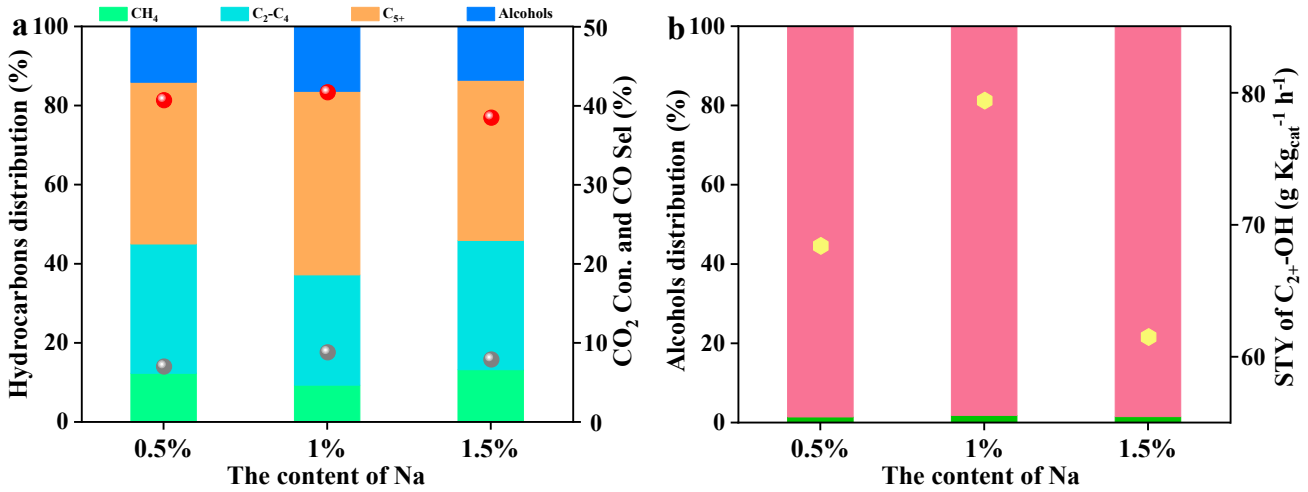

Supplementary Figure 3. The catalytic performance of CO_2 hydrogenation under different Na content. a CO_2 hydrogenation performance of $FeTiO_x$ under different Na contents. **b** Percentage of higher alcohols in the alcohol and the STY of higher alcohols for $FeTiO_x$ under different Na contents. Reaction conditions: 5.0 MPa, 320 °C, feed gas (Ar 5 vol%, CO_2 27 vol%, H_2 68 vol%), GHSV = 4800 mL g_{cat}^{-1} h^{-1}.

Note:

An appropriate amount of Na promoter can effectively enhance both catalytic activity and alcohol selectivity. The catalytic performance and alcohol selectivity of catalysts with different Na loadings are shown in Supplementary Figure 3 and Supplementary Table 1. As the Na loading increased, both CO_2 conversion and alcohol/higher alcohols selectivity initially increased and then gradually decreased. This trend suggests that optimal Na loading is beneficial for promoting higher alcohols synthesis, whereas excessive Na incorporation may partially cover the active sites of the catalyst, thereby hindering reactant adsorption and intermediate conversion. Consequently, excessive Na loading leads to decreased CO_2 conversion and reduced selectivity toward higher alcohols.

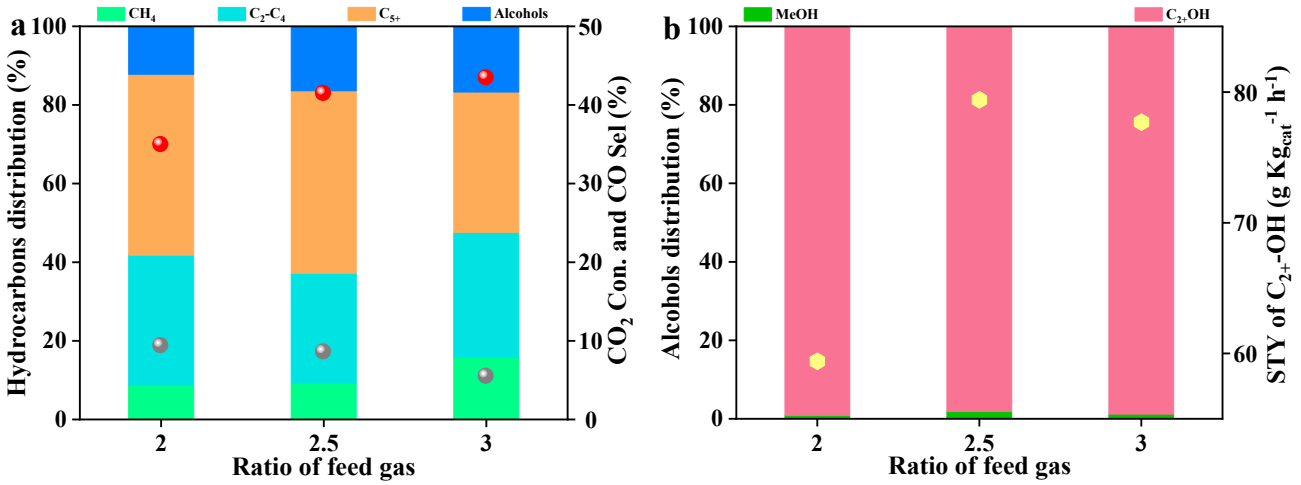

Supplementary Figure 4. The Catalytic performance of CO_2 hydrogenation under different feed gas. a CO_2 hydrogenation performance of 1%Na-$FeTiO_x$ under different feed gas (H_2/CO_2=2.0: Ar 4 vol%, CO_2 32 vol%, H_2 64 vol%. H_2/CO_2=2.5: Ar 5 vol%, CO_2 27 vol%, H_2 68 vol%. H_2/CO_2=3.0: Ar 4 vol%, CO_2 24 vol%, H_2 72 vol%.). **b** Percentage of higher alcohols in the alcohol and the STY of higher alcohols for $FeTiO_x$ under different feed gas (H_2/CO_2=2.0: Ar 4 vol%, CO_2 32 vol%, H_2 64 vol%. H_2/CO_2=2.5: Ar 5 vol%, CO_2 27 vol%, H_2 68 vol%. H_2/CO_2=3.0: Ar 4 vol%, CO_2 24 vol%, H_2 72 vol%.). Reaction conditions: 5.0 MPa, 320 °C, GHSV = 4800 mL g_{cat}^{-1} h^{-1}.

Note:

The H_2/CO_2 ratio in the feed gas plays a critical role in determining both CO_2 conversion and product distribution during CO_2 hydrogenation. To further evaluate the catalytic performance of 1%Na-$FeTiO_x$ toward higher alcohols synthesis, the influence of the H_2/CO_2 ratio was systematically investigated. As shown in Supplementary Figure 4 and Supplementary Table 2, increasing the H_2/CO_2 ratio led to enhanced CO_2 conversion, accompanied by improved selectivity toward alcohols, particularly higher alcohols, over the 1%Na-$FeTiO_x$ catalyst. Although a H_2/CO_2 ratio of 3 resulted in slightly higher CO_2 conversion and superior higher alcohols selectivity, considering the relative CO_2 concentration in the feed gas and the space-time yield (STY) of higher alcohols, a H_2/CO_2 ratio of 2.5 was ultimately considered more suitable for efficient higher alcohols production from CO_2 over this catalytic system.

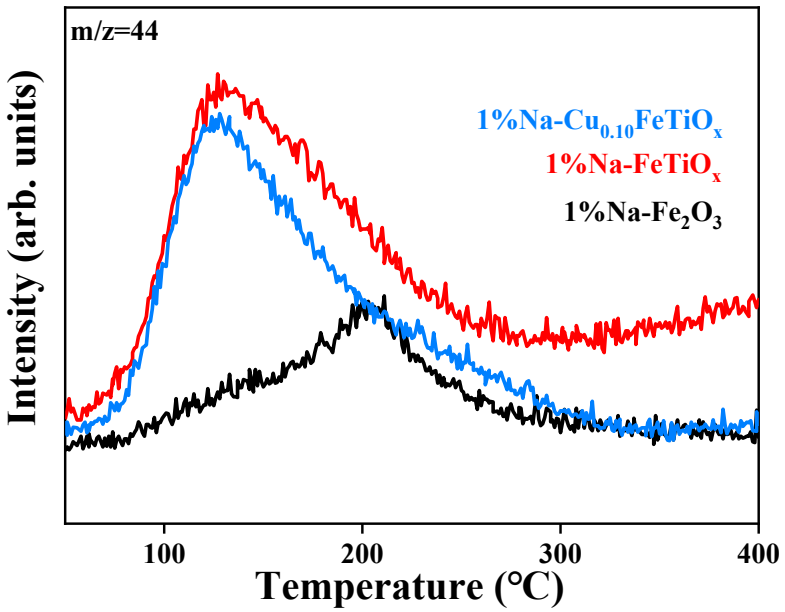

Supplementary Figure 5. The results of CO_2-TPD for different catalysts. CO_2-TPD spectra of 1%Na-Fe_2O_3, 1%Na-$FeTiO_x$ and 1%Na-$Cu_{0.10}FeTiO_x$.

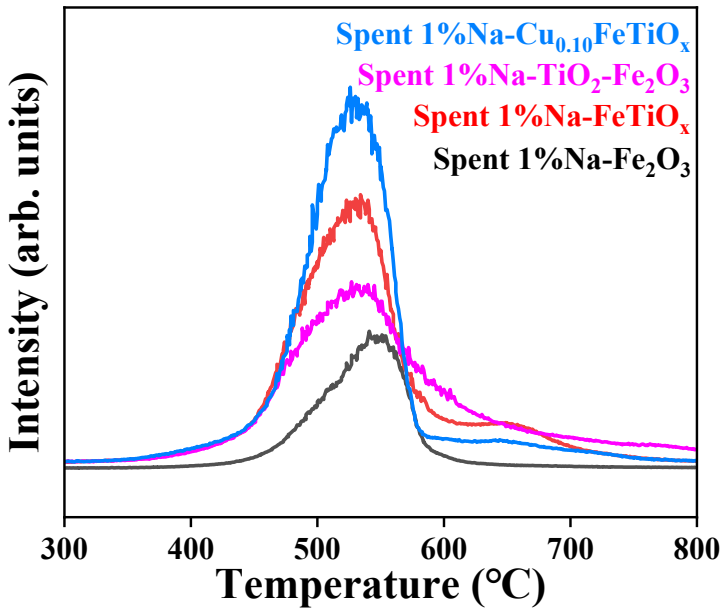

Supplementary Figure 6. The results of CO-TPD for different catalysts. CO-TPD spectra of spent 1%Na-Fe_2O_3,1%Na-$FeTiO_x$, 1%Na-TiO_2-Fe_2O_3 and 1%Na-$Cu_{0.10}FeTiO_x$.

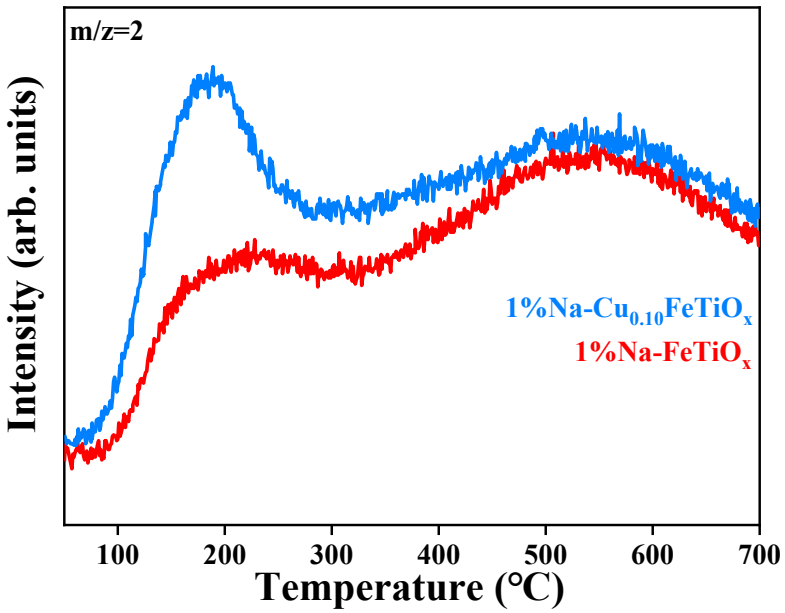

Supplementary Figure 7. The results of H_2-TPD for different catalysts. H_2-TPD spectra of 1%Na-$FeTiO_x$ and 1%Na-$Cu_{0.10}FeTiO_x$.

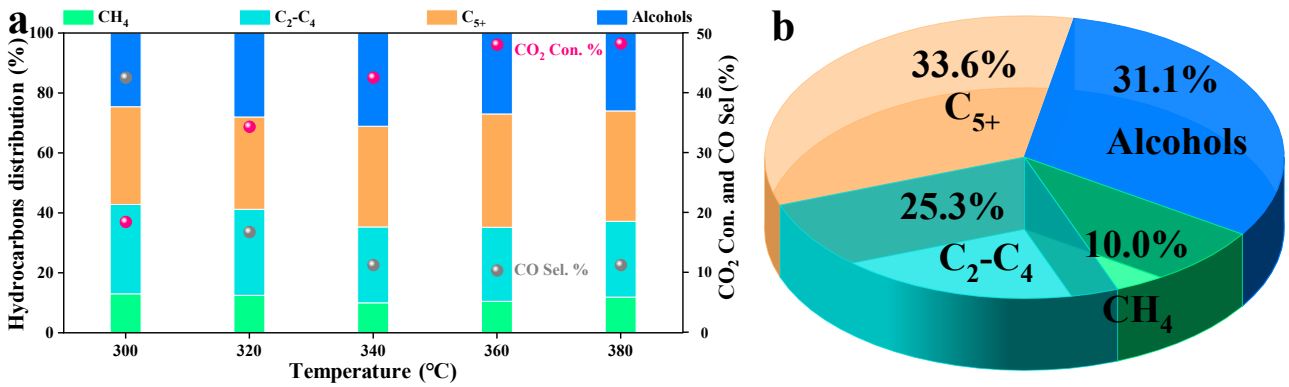

Supplementary Figure 8. The catalytic performance of CO_2 hydrogenation under different temperatures. **a** CO_2 hydrogenation performance of 1% Na-$Cu_{0.10}FeTiO_x$ under different temperatures. Reaction conditions: 5.0 MPa, CO_2: H_2 =1:2.5, GHSV = 8000 mL $gcat^{-1}$ h^{-1}. **b** Product distribution excluding CO of CO_2 hydrogenation at 340 °C for 1% Na-$Cu_{0.10}FeTiO_x$. Reaction conditions: 5.0 MPa, 340 °C, feed gas (Ar 5 vol%, CO_2 27 vol%, H_2 68 vol%), GHSV = 8000 mL g_{cat}^{-1} h^{-1}.

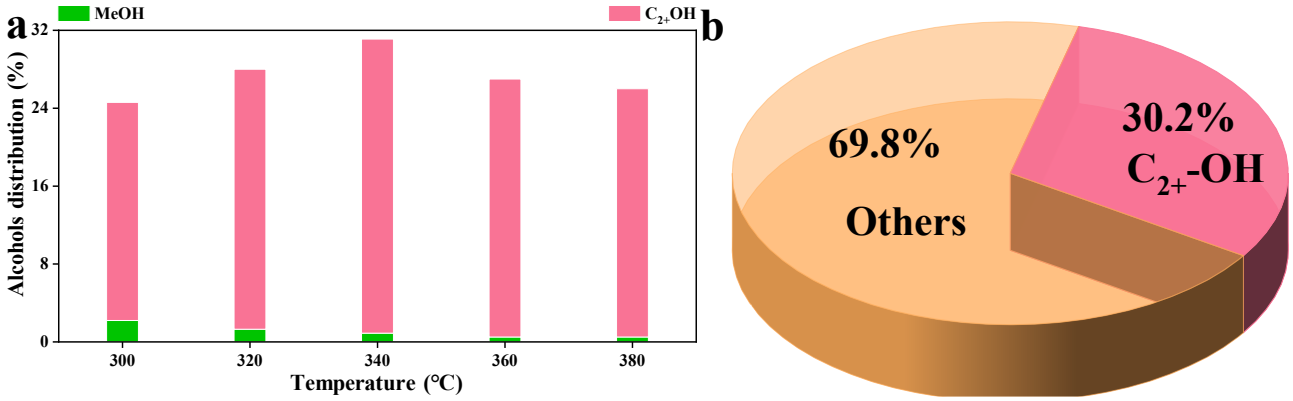

Supplementary Figure 9. The catalytic performance of CO_2 hydrogenation under different temperatures. a Alcohol distribution of 1% Na-$Cu_{0.10}FeTiO_x$ under different temperatures. Reaction conditions: 5.0 MPa, CO_2: H_2 =1:2.5, GHSV = 8000 mL $gcat^{-1}$ h^{-1}. **b** Percentage of alcohols excluding CO for 1% Na-$Cu_{0.10}FeTiO_x$ at 340 °C. Reaction conditions: 5.0 MPa, 340 °C, feed gas (Ar 5 vol%, CO_2 27 vol%, H_2 68 vol%), GHSV = 8000 mL g_{cat}^{-1} h^{-1}.

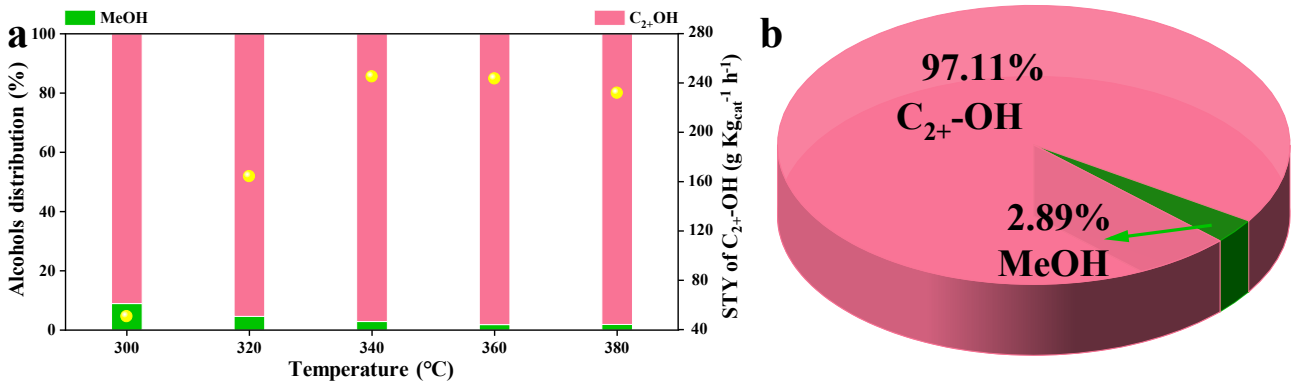

Supplementary Figure 10. The catalytic performance of CO_2 hydrogenation under different temperatures. a Percentage of higher alcohols in the alcohol and the STY of higher alcohols for different iron-based catalysts. Reaction conditions: 5.0 MPa, CO_2: H_2 =1:2.5, GHSV = 8000 mL g_{cat}^{-1} h^{-1}. **b** Percentage of different alcohols in the alcohol phase of 1% Na-$Cu_{0.10}FeTiO_x$ at 340 °C. Reaction conditions: 5.0 MPa, 340 °C, feed gas (Ar 5 vol%, CO_2 27 vol%, H_2 68 vol%), GHSV = 8000 mL g_{cat}^{-1} h^{-1}.

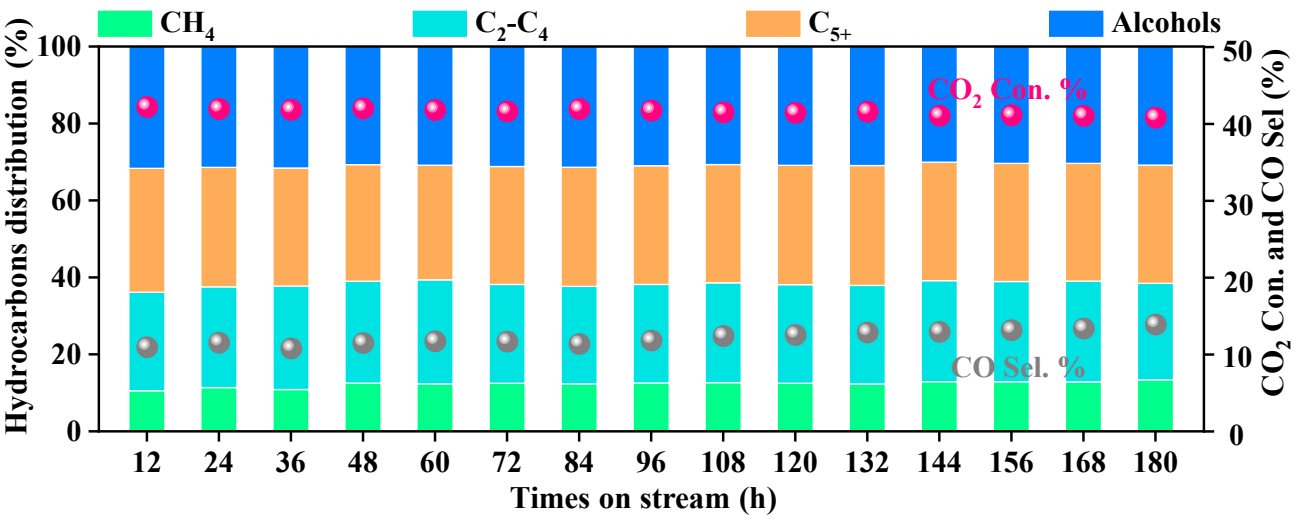

Supplementary Figure 11. The catalytic stability of CO_2 hydrogenation for 1%Na-$Cu_{0.10}FeTiO_x$.

Catalytic stability of 1%Na-$Cu_{0.10}FeTiO_x$ catalyst for CO_2 hydrogenation. Reaction conditions: 5.0 MPa, 340 °C, feed gas (Ar 5 vol%, CO_2 27 vol%, H_2 68 vol%), GHSV = 8000 mL g_{cat}^{-1} h^{-1}.

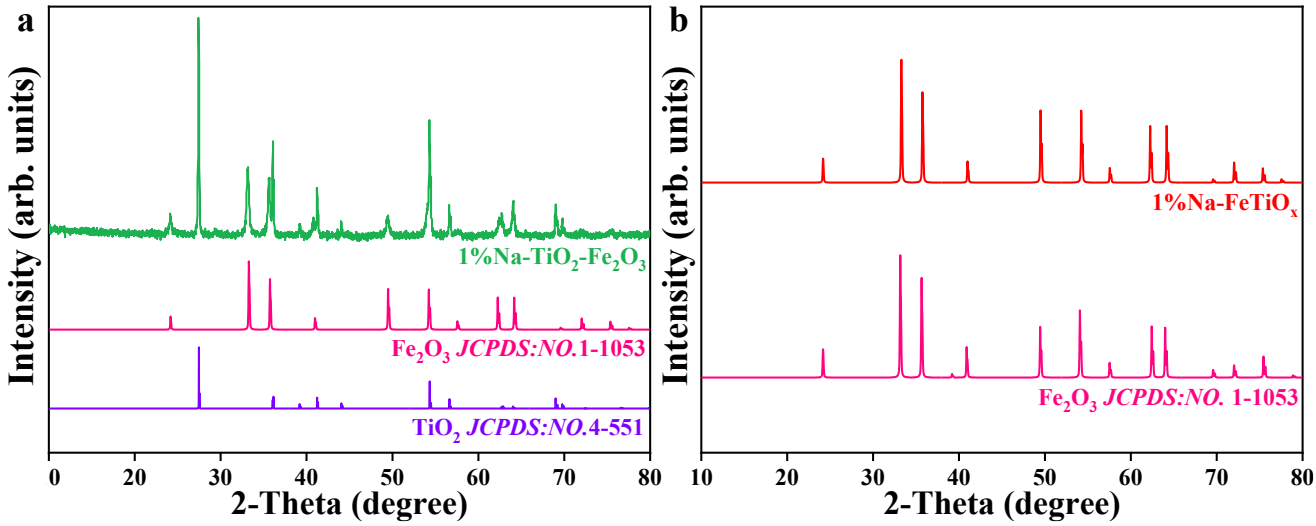

Supplementary Figure 12. The phase structure of 1% Na-TiO_2-Fe_2O_3 and 1%Na-$FeTiO_X$. XRD patterns of 1%Na-TiO_2-Fe_2O_3 (a) and 1%Na-$FeTiO_x$ (b).

Note:

The phase structure of the fresh catalyst 1%Na-TiO_2-Fe_2O_3 and 1%Na-$FeTiO_x$ was characterized using X-ray diffraction (XRD). As illustrated in Supplementary Figure 12b, the phase structure of the 1%Na-$FeTiO_x$ catalyst corresponds to hematite (Fe_2O_3, ***JCPDS No.*** 1-1053) after high-temperature calcination and alkali metal impregnation. In contrast, the 1% Na-TiO_2-Fe_2O_3 sample shown in Supplementary Figure 12a consists of two phases: TiO_2 and Fe_2O_3. This result indicates that the synthesized 1%Na-$FeTiO_x$ does not contain any phase structures corresponding to metallic titanium or titanium oxides.

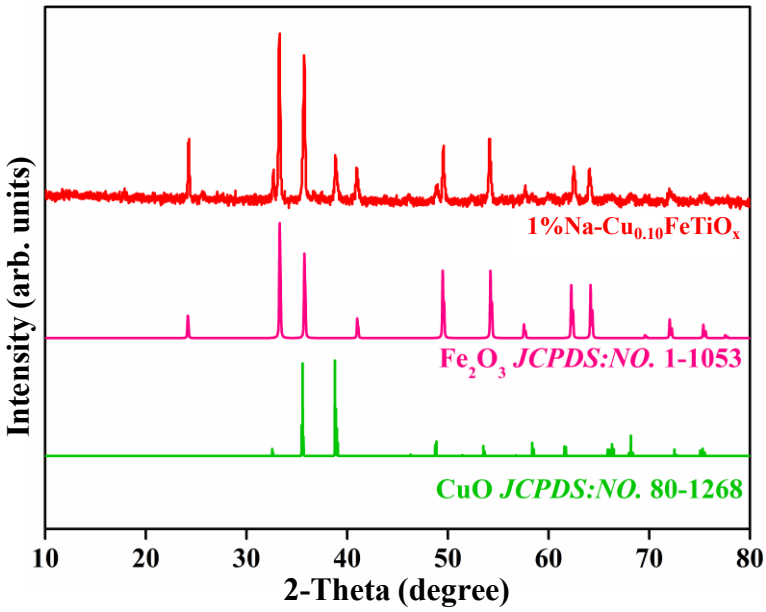

Supplementary Figure 13. The phase structure of 1%Na-$Cu_{0.10}FeTiO_x$. XRD patterns of 1%Na-$Cu_{0.10}FeTiO_x$.

Note:

The phase structure of the fresh catalyst 1%Na-$Cu_{0.10}FeTiO_x$ was analyzed by XRD. As depicted in Supplementary Figure 13, the incorporation of copper did not alter the hematite phase structure of $FeTiO_x$ (Fe_2O_3, ***JCPDS No.*** 1-1053). Meanwhile, it successfully facilitated the introduction of the monoclinic phase of CuO (***JCPDS No.*** 80-1268), indicating that copper was effectively integrated into the $FeTiO_x$ structure.

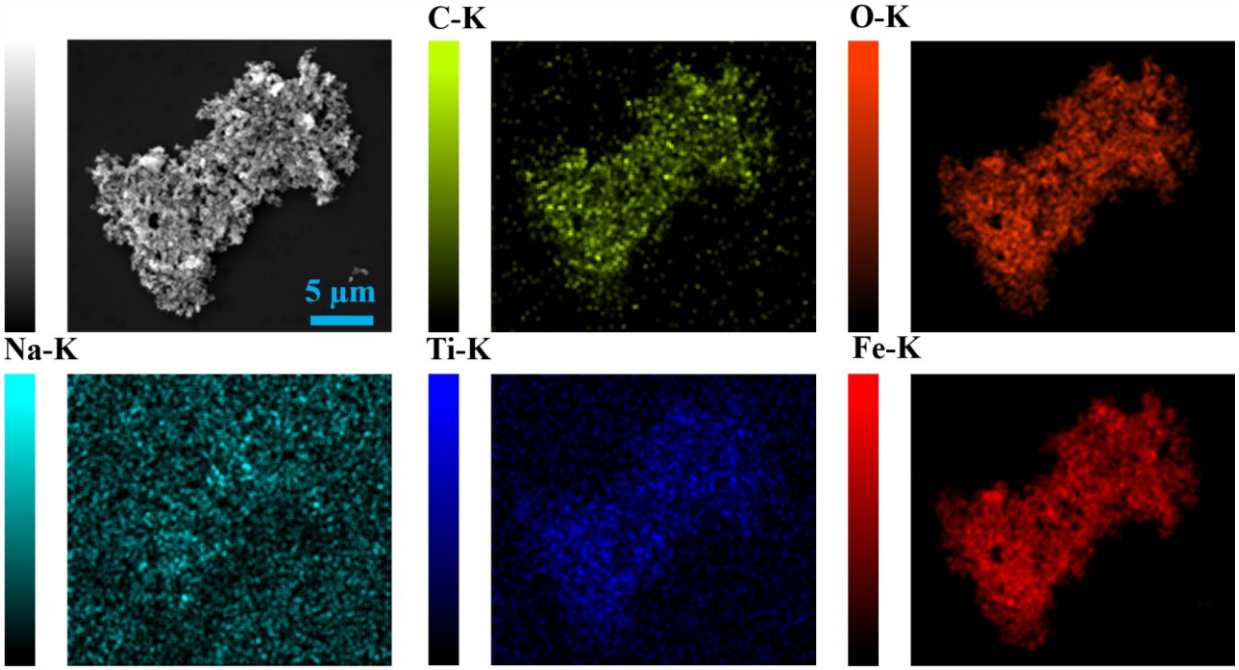

Supplementary Figure 14. The morphological characteristics and element distribution of 1%Na-FeTiO$_x$. SEM and SEM-Mapping of 1%Na-FeTiO$_x$.

Note:

The morphological characteristics and elemental distribution of the catalyst, 1%Na-FeTiO$_x$, are illustrated in Supplementary Figure 14, revealing a highly uniform dispersion of all metal components. Notably, the distribution regions of titanium (Ti) closely align with those of iron (Fe), oxygen (O), and carbon (C), suggesting that titanium is retained within the structure. Furthermore, an amorphous form of Ti metal can be inferred based on the XRD analysis results.

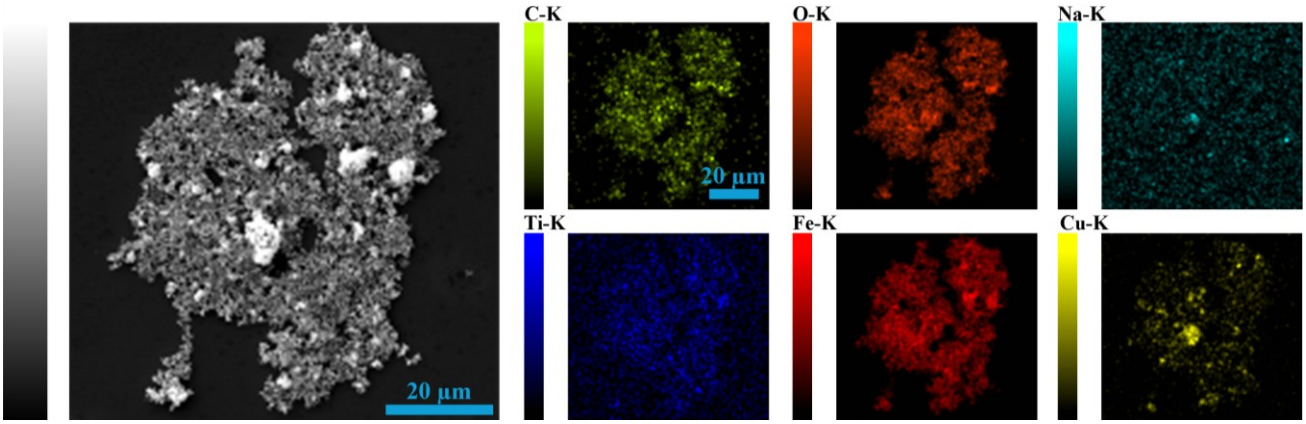

Supplementary Figure 15. The morphological characteristics and element distribution of 1%Na-$Cu_{0.10}FeTiO_x$. SEM and SEM-Mapping of 1%Na-$Cu_{0.10}FeTiO_x$.

Note:

The morphological features and elemental distributions of the 1%Na-$Cu_{0.10}FeTiO_x$ catalyst (Supplementary Figure 15) reveal that all metallic components are highly and uniformly dispersed. Notably, the spatial distribution of Ti closely mirrors that of Fe, O and C, indicating the successful incorporation of Ti into the catalyst matrix. Copper signals are also clearly detected and are largely homogeneous across the observed regions, although minor local aggregation is present. Similarly, combined with the XRD results, it can be inferred that Ti metal may exist in an amorphous form.

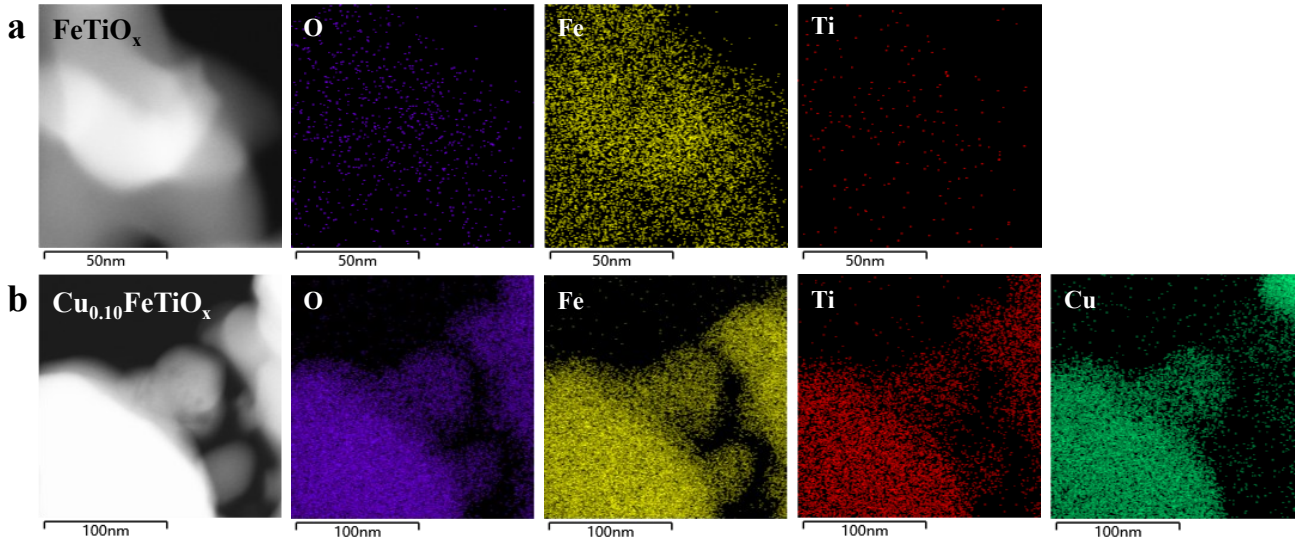

Supplementary Figure 16. The microscopic morphological characteristics and element distribution of $FeTiO_x$ and $Cu_{0.10}FeTiO_x$. TEM and TEM-Mapping of $FeTiO_x$ (a) and $Cu_{0.10}FeTiO_x$ (b).

Note:

To further investigate the microscopic distribution of the metallic species, TEM elemental mapping analyses were performed for the above two catalysts. As shown in Supplementary Figure 16a, Fe and Ti species in $FeTiO_x$ exhibit a relatively homogeneous spatial distribution, which is consistent with the observed morphological features of the catalyst. Similarly, in $Cu_{0.10}FeTiO_x$, Fe, Cu, and Ti species remain uniformly distributed throughout the catalyst matrix, in good agreement with the corresponding microscopic morphology of $Cu_{0.10}FeTiO_x$ (Supplementary Figure 16b).

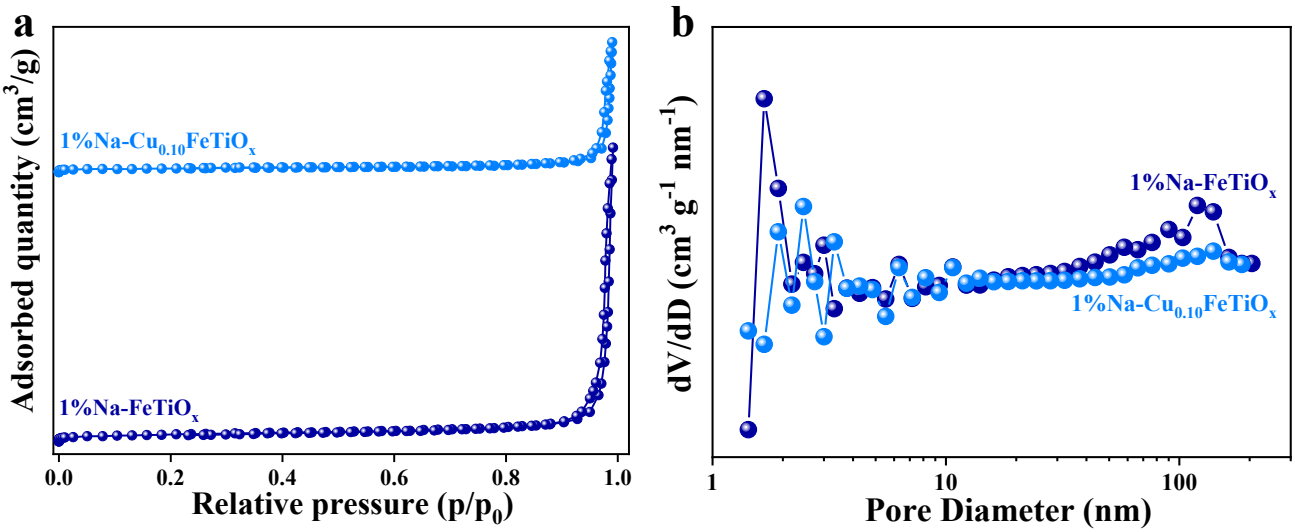

Supplementary Figure 17. The results of BET for 1%Na-FeTiO$_x$ and 1%Na-Cu$_{0.10}$FeTiO$_x$. a N_2 adsorption-desorption isotherms of 1%Na-FeTiO$_x$ and 1%Na-Cu$_{0.10}$FeTiO$_x$. **b** Pore size distributions of 1%Na-FeTiO$_x$ and 1%Na-Cu$_{0.10}$FeTiO$_x$.

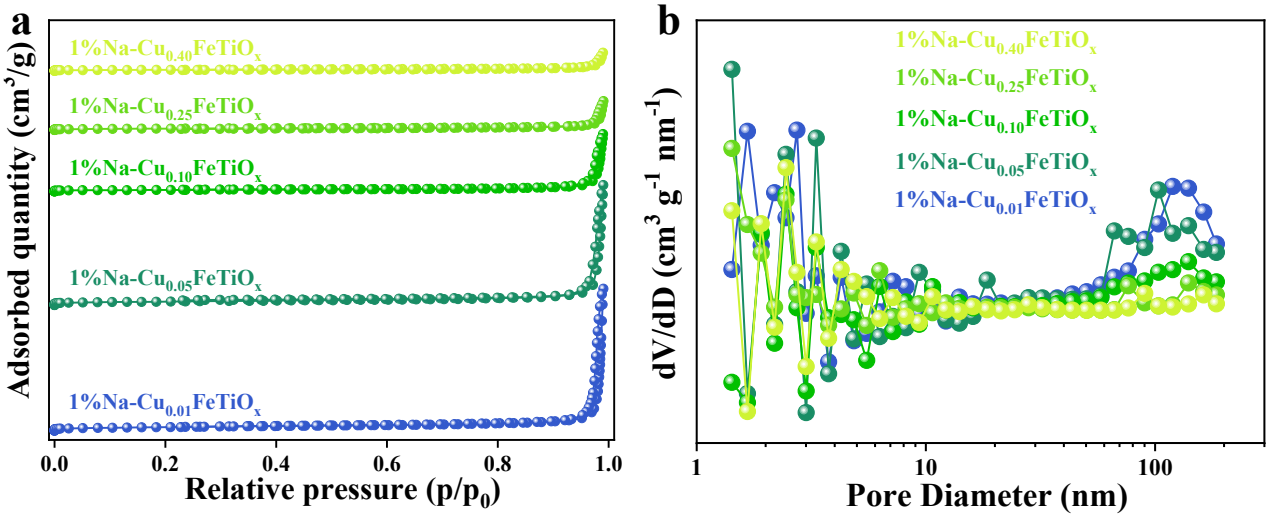

Supplementary Figure 18. The results of BET for different catalysts. a N_2 adsorption-desorption isotherms of 1%Na-$FeTiO_x$ with different Cu doping amounts. **b** Pore size distributions of 1%Na-$FeTiO_x$ with different Cu doping amounts.

Note:

The nitrogen adsorption-desorption isotherms, specific surface area, pore size distribution, and pore volume of all catalysts are shown in Supplementary Figure 17 and Supplementary Figure 18 and Supplementary Table 6. The analysis results show that the introduction of even a very small amount of Cu metal can increase the average pore size, void volume, and specific surface area of $FeTiO_x$. However, continuous introduction of Cu metal will further lead to a rapid decrease in the average pore size, void volume, and specific surface area of $FeTiO_x$.

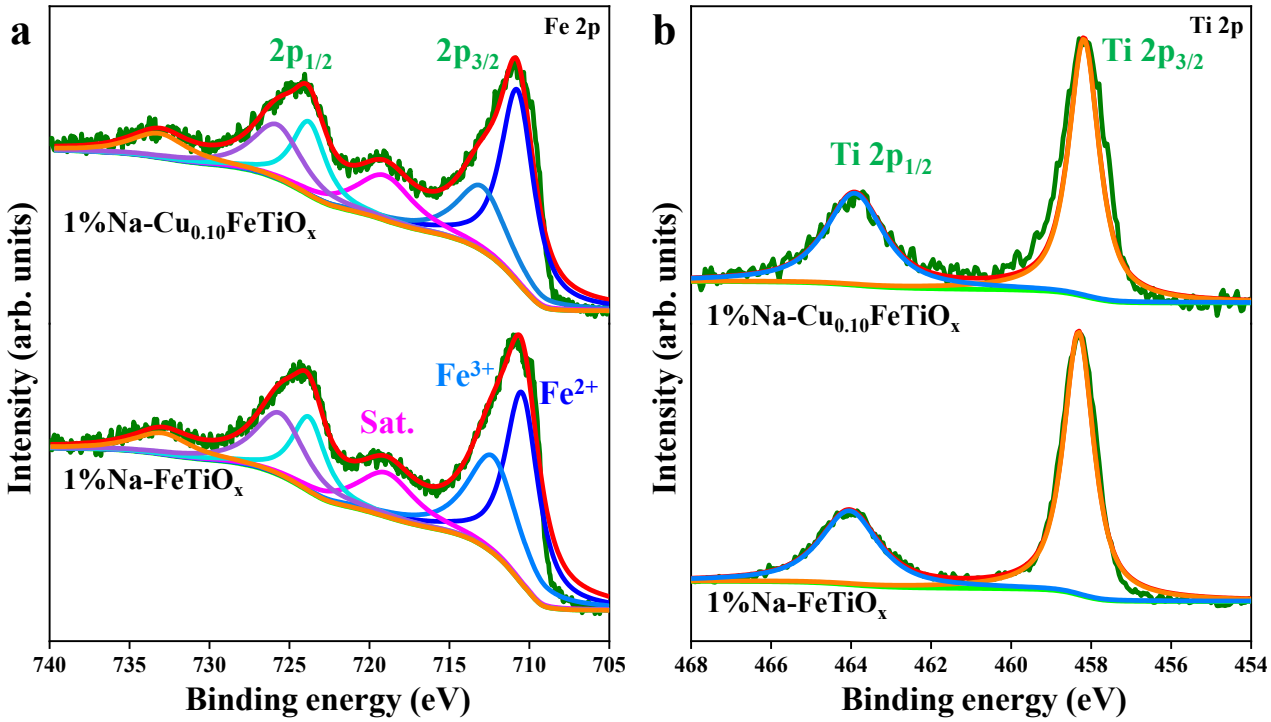

Supplementary Figure 19. The results of Fe 2*p* and Ti 2*p* XPS fine spectra for fresh catalysts. **a** Fe 2*p* XPS fine spectra of 1%Na-$FeTiO_x$ and 1%Na-$Cu_{0.10}FeTiO_x$. **b** Ti 2*p* XPS fine spectra of 1%Na-$FeTiO_x$ and 1%Na-$Cu_{0.10}FeTiO_x$.

Note:

The high-resolution Fe 2*p* fine spectra of 1%Na-$FeTiO_x$ and 1%Na-$Cu_{0.10}FeTiO_x$ were deconvoluted into six characteristic peaks, respectively (Supplementary Figure 19a). The binding energies at 710.59, 712.53 and 719.23 eV are assigned to Fe^{2+}, Fe^{3+} and the satellite peak in the Fe $2p_{3/2}$ region, respectively. Additionally, the binding energies at 723.92, 725.82 and 733.14 eV are assigned to Fe^{2+}, Fe^{3+} and the satellite feature in the Fe $2p_{1/2}$ region, respectively. Supplementary Figure 19b shows the high-resolution Ti 2*p* XPS fine spectra of 1%Na-$FeTiO_x$ and 1%Na-$Cu_{0.10}FeTiO_x$, where the characteristic peaks at 458.31 and 464.06 eV are assigned to Ti $2p_{3/2}$ and Ti $2p_{1/2}$, respectively.

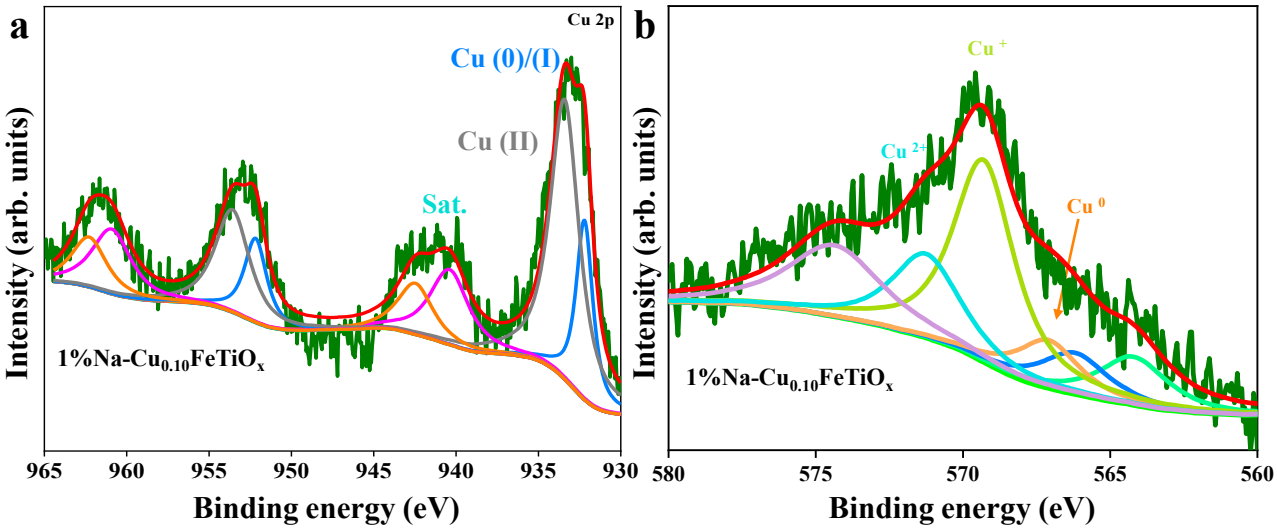

Supplementary Figure 20. The results of Cu 2*p* and Cu LMM XPS fine spectra for fresh catalysts.

a Cu 2*p* XPS fine spectra of 1%Na-$Cu_{0.10}FeTiO_x$. **b** Cu LMM XPS fine spectra of 1%Na-$Cu_{0.10}FeTiO_x$.

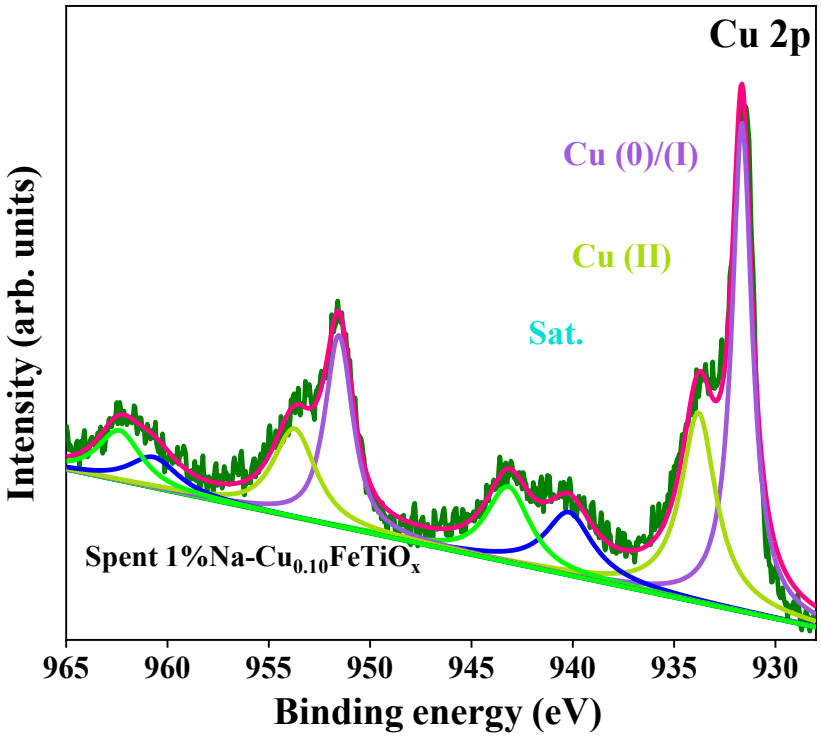

Supplementary Figure 21. The results of Cu 2*p* XPS fine spectra for spent 1%Na-$Cu_{0.10}FeTiO_x$.

Cu 2*p* XPS fine spectra of spent 1%Na-$Cu_{0.10}FeTiO_x$.

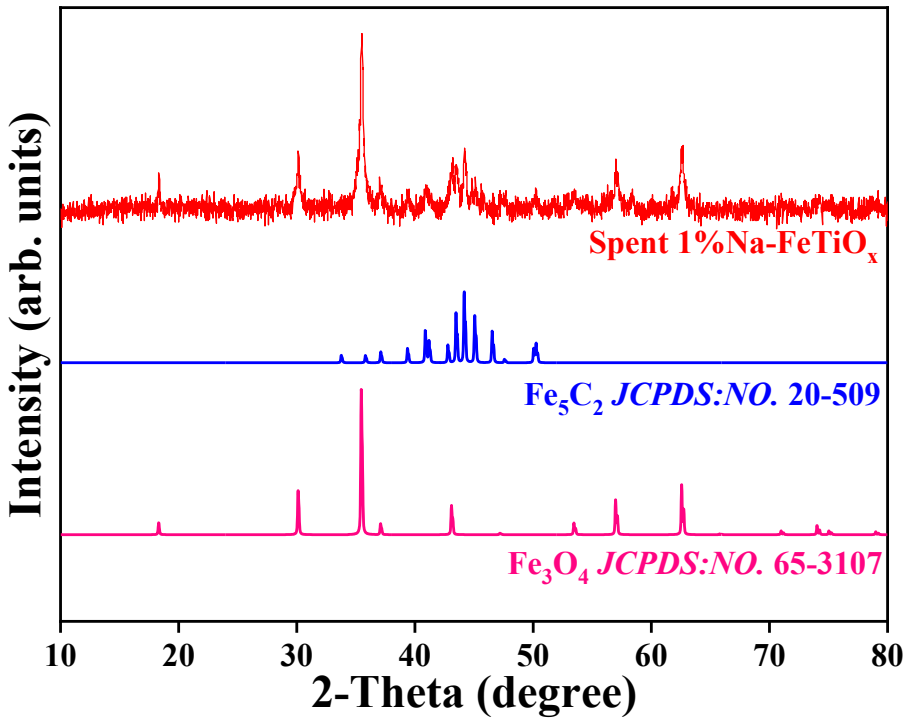

Supplementary Figure 22. The phase structure of spent 1%Na-FeTiO$_X$. XRD patterns of spent 1%Na-FeTiO$_x$.

Supplementary Table 1 Catalytic performances of different iron-based catalysts.

Catalyst	CO_2 Conv. (%)	T (°C)	P (MPa)	CO Sel. (%)	Selectivity (%)					
					CH_4	$C_{2-4}^{=}$	C_{2-4}^{p}	C_5^+	O_{xy} (C_2^+-OH)	STY(C_2^+-OH) $g \cdot kg_{cat}^{-1} \cdot h^{-1}$
1%Na-Fe_2O_3	31.5	320	5.0	11.5	12.6	30.8	6.8	44.2	5.6 (5.4)	20.0
1%Na-TiO_2-Fe_2O_3	39.1	320	5.0	4.4	9.5	21.7	5.6	51.5	11.7(11.5)	56.1
0.5%Na-$FeTiO_x$	40.7	320	5.0	7.0	12.3	24.8	7.9	40.9	14.1 (13.9)	68.4
1%Na-$FeTiO_x$	41.7	320	5.0	8.8	9.3	22.0	5.9	46.4	16.4 (16.1)	79.4
1.5%Na-$FeTiO_x$	38.5	320	5.0	7.9	13.2	25.7	7.0	40.5	13.6 (13.4)	61.5
1%Na-$Cu_{0.01}FeTiO_x$	41.5	320	5.0	9.2	9.4	21.5	6.0	44.3	18.8 (18.3)	89.7
1%Na-$Cu_{0.05}FeTiO_x$	41.0	320	5.0	10.6	10.8	21.0	7.4	36.6	24.2 (23.3)	110.8
1%Na-$Cu_{0.10}FeTiO_x$	39.0	320	5.0	12.8	10.9	19.6	7.7	33.8	28.0 (26.9)	118.4
1%Na-$Cu_{0.25}FeTiO_x$	39.0	320	5.0	12.8	11.1	23.0	6.6	33.4	25.9 (24.7)	108.7
1%Na-$Cu_{0.40}FeTiO_x$	35.6	320	5.0	16.9	12.9	21.3	9.4	30.8	25.6 (24.4)	93.5

Reaction conditions: 5.0 MPa, 320 °C, feed gas (Ar 5 vol%, CO_2 27 vol%, H_2 68 vol%), TOS = 8 h, GHSV = 4800 mL g_{cat}^{-1} h^{-1}.

Supplementary Table 2 Catalytic performances of different iron-based catalysts.

Catalyst	CO_2 Conv. (%)	Ratio of feed gas	P (MPa)	CO Sel. (%)	Selectivity (%)					
					CH_4	$C_{2\text{-}4}^{=}$	$C_{2\text{-}4}^{p}$	C_5^+	O_{xy} (C_2^+-OH)	STY(C_2^+-OH) $g \cdot kg_{cat}^{-1} \cdot h^{-1}$
[a]1%Na-$FeTiO_x$	39.3	2.5	3.0	5.3	12.3	24.5	8.7	40.0	14.5 (13.5)	65.2
	40.8	2.5	4.0	6.9	10.9	21.2	7.2	45.2	15.6 (15.3)	76.2
	41.7	2.5	5.0	8.8	9.3	22.0	5.9	46.4	16.4 (16.1)	79.4
[b]1%Na-$FeTiO_x$	35.2	2.0	5.0	9.6	8.8	28.0	5.0	46.0	12.1(12.0)	59.4
	41.7	2.5	5.0	8.8	9.3	22.0	5.9	46.4	16.4(16.1)	79.4
	43.7	3.0	5.0	5.7	15.8	21.5	10.3	35.7	16.7(16.5)	77.7

a: Reaction conditions: 320 °C, feed gas (H_2/CO_2=2.5: Ar 5 vol%, CO_2 27 vol%, H_2 68 vol%.), different pressure (3.0, 4.0 and 5.0 MPa), TOS = 8 h, GHSV = 4800 mL g_{cat}^{-1} h^{-1}.

b: Reaction conditions: 320 °C, different feed gas (H_2/CO_2=2.0: Ar 4 vol%, CO_2 32 vol%, H_2 64 vol%. H_2/CO_2=2.5: Ar 5 vol%, CO_2 27 vol%, H_2 68 vol%. H_2/CO_2=3.0: Ar 4 vol%, CO_2 24 vol%, H_2 72 vol%.), 5.0 MPa, TOS = 8 h, GHSV = 4800 mL g_{cat}^{-1} h^{-1}.

Supplementary Table 3 Catalytic performances of 1%Na-$Cu_{0.10}FeTiO_x$ under different space velocities.

GHSV (mL g_{cat}^{-1} h^{-1})	CO_2 Conv. (%)	T (°C)	P (MPa)	CO Sel. (%)	Selectivity (%)					
					CH_4	$C_{2-4}^{=}$	C_{2-4}^{p}	C_5^+	O_{xy} (C_2^+-OH)	STY(C_2^+-OH) $g \cdot kg_{cat}^{-1} \cdot h^{-1}$
4800	39.0	320	5.0	12.8	10.9	19.6	7.7	33.8	28.0 (26.9)	118.4
6000	36.3	320	5.0	14.7	11.2	21.7	7.6	31.3	28.2 (27.2)	136.3
8000	34.3	320	5.0	16.7	12.5	20.3	8.4	30.8	28.0 (26.7)	164.5
12000	30.1	320	5.0	21.2	13.3	22.0	10.5	31.2	23.0 (22.0)	169.1
24000	25.4	320	5.0	25.1	14.7	23.7	11.2	29.2	21.2 (20.3)	249.7

Reaction conditions: 5.0 MPa, 320 °C, feed gas (Ar 5 vol%, CO_2 27 vol%, H_2 68 vol%), TOS = 8 h.

Supplementary Table 4 Catalytic performances of 1%Na-$Cu_{0.10}FeTiO_x$ under different temperatures.

Temperature (℃)	CO_2 Conv. (%)	P (MPa)	CO Sel. (%)	Selectivity (%)					
				CH_4	$C_{2-4}^{=}$	C_{2-4}^{P}	C_5^+	O_{xy} (C_2^+-OH)	STY(C_2^+-OH) $g \cdot kg_{cat}^{-1} \cdot h^{-1}$
300	18.4	5.0	42.5	13.0	22.2	7.6	32.6	24.6 (22.4)	50.9
320	34.3	5.0	16.7	12.5	20.3	8.4	30.8	28.0 (26.7)	164.5
340	42.5	5.0	11.2	10.0	19.3	6.0	33.6	31.1 (30.2)	245.4
360	48.0	5.0	10.3	10.5	19.9	4.8	37.8	27.0 (26.5)	243.7
380	48.2	5.0	11.2	11.9	19.8	5.5	36.8	26.0 (25.5)	232.1

Reaction conditions: 5.0 MPa, feed gas (Ar 5 vol%, CO_2 27 vol%, H_2 68 vol%), TOS = 8 h, GHSV = 8000 mL g_{cat}^{-1} h^{-1}.

Supplementary Table 5. Catalytic results of various Fe-based catalysts for CO_2 hydrogenation to higher alcohols.

Catalysts	T (ºC)	P (MPa)	GHSV (mL g^{-1} cat h^{-1})	CO_2 Conv./%	C_2^+OH Sel./%	C_2^+OH STY (mg g^{-1} cat h^{-1})	Ref.
1%Na-$Cu_{0.10}FeTiO_x$	340	5.0	8000	42.5	30.2	245.4	**This work**
CuFe	320	3.0	6000	34.7	12.7	34.0	[1]
K-CuZnAl/Zr-CuFe	320	4.0	24000	26.0	20.0	195.1	[2]
CuZnAl/K-uMgZnFe	320	5.0	6000	42.3	17.4	106.5	[3]
4.6K-CuMgZnFe	320	5.0	6000	30.4	15.9	69.6	[4]
KFeCu/a-ZrO_2	320	4.0	9000	27.8	27.0	118.2	[5]
Na-ZnFe@C	320	5.0	9000	38.4	24.5	158.1(EtOH)	[6]
NaS-10FeCu	320	3.0	8000	35.7	18.7	108	[7]
$NiFe_2O_4/Fe_2O_3$	330	3.0	24000	25.5	17.0	190.1(EtOH)	[8]
PdFe-6.9	320	5.0	6000	35.6	23.0	87.8	[9]
Na-Fe@C/K-CuZnAl	320	5.0	4500	39.2	40.9	＞158.5	[10]
Cs-CuFeZn	330	5.0	4500	36.6	19.8	73.4	[11]
Cr(1%)-CuFe	320	4.0	6000	38.4	29.2	104.1	[12]
$2Na/Fe_1Cu_2Mg_1$	380	5.0	4500	55.4	10.2	110.1	[13]
$ZnFe_2O_4$/Fe-Zn-Na#	320	5.0	12000	29.1	18.6	137.7	[14]
FeCo&CZA	320	5.0	4500	55.5	42.4	236.8	[15]
KFeCuZr-1.6	300	4.5	6000	28.2	12.02	51.83	[16]
1Pd/2Na/α-Fe_2O_3	300	5.0	3000	31.2	32.2	82.8	[17]
$CuZnFeO_x$	340	5.0	6000	35.2	28.9	125.1	[18]

Supplementary Table 6 The Mean pore size, Pore volume and S_{BET} of different catalysts.

Catalyst	Mean pore size /nm	Pore volume /cm^3 g^{-1}	S_{BET} /m^2 g^{-1}
1%Na-$FeTiO_x$	64.64	2.49	10.84
1%Na-$Cu_{0.01}FeTiO_x$	62.90	2.92	12.71
1%Na-$Cu_{0.05}FeTiO_x$	57.13	2.73	11.96
1%Na-$Cu_{0.10}FeTiO_x$	53.90	1.22	5.30
1%Na-$Cu_{0.25}FeTiO_x$	34.16	1.06	4.62
1%Na-$Cu_{0.40}FeTiO_x$	29.60	0.83	3.61

Supplementary References

[1] Qixin Fan, Na Liu, Jingming Zhao, Yang Yu, Yannan Sun, Yu Han, Jixin Zhang, Aimin Wang, Qingjie Ge, Jian Wei, Jian Sun, Regulating the location of metal promoters in CuFe-based catalysts for enhanced CO_2 hydrogenation to higher alcohols, Journal of Energy Chemistry, 107, 2025, 31-43.

[2] Qian Zhang, Sen Wang, Xuerong Shi, Mei Dong, Jiangang Chen, Juan Zhang, Jianguo Wang, Weibin Fan, Conversion of CO_2 to higher alcohols on K-CuZnAl/Zr-CuFe composite, Applied Catalysis B: Environment and Energy, 346, 2024, 123748.

[3] Di Xu, Hengquan Yang, Xinlin Hong, Guoliang Liu, Shik Chi Edman Tsang, Tandem Catalysis of Direct CO_2 Hydrogenation to Higher Alcohols, ACS Catalysis, 11, 2021, 8978-8984.

[4] Di Xu, Mingyue Ding, Xinlin Hong, Guoliang Liu, Mechanistic Aspects of the Role of K Promotion on Cu-Fe-Based Catalysts for Higher Alcohol Synthesis from CO_2 Hydrogenation, ACS Catalysis, 10, 2020, 14516-14526.

[5] Tangkang Liu, Di Xu, Mengyang Song, Xinlin Hong, Guoliang Liu, K-ZrO_2 Interfaces Boost CO_2 Hydrogenation to Higher Alcohols, ACS Catalysis, 13, 2023, 4667-4674.

[6] Yang Wang, Wenhang Wang, Ruosong He, Meng Li, Jinqiang Zhang, Fengliang Cao, Jianxin Liu, Shiyuan Lin, Xinhua Gao, Guohui Yang, Mingqing Wang, Tao Xing, Tao Liu, Qiang Liu, Han Hu, Noritatsu Tsubaki, Mingbo Wu, Carbon-Based Electron Buffer Layer on ZnO_x-Fe_5C_2-Fe_3O_4 Boosts Ethanol Synthesis from CO_2 Hydrogenation, Angewandte Chemie International Edition, 62, 2023, e202311786.

[7] Ruwei Yao, Yang Yu, Bin Wu, Yueyin Song, Qinqin Niu, Congming Li, Jian Wei, Qingjie Ge, Synergistic Na-S modified Fe-Cu catalysts for efficient CO_2 hydrogenation to higher alcohols, Chemical Engineering Journal, 512, 2025, 162498.

[8] Wenjie Xiang, Shuhei Yasuda, Lijun Zhang, Jiaqi Fan, Kazuki Tsukamoto, Yue Xin, Noritatsu Tsubaki, $NiFe_2O_4$ spinel engineering for transcending the dilemma of activity-selectivity in CO_2 hydrogenation to ethanol, Nature Communications, 17, 2026, 572.

[9] Yanqiu Wang, Ying Zhou, Xinxin Zhang, Mingrui Wang, Tangkang Liu, Jinxing Wei, Guanghui Zhang, Xinlin Hong, Guoliang Liu, PdFe alloy-Fe_5C_2 interfaces for efficient CO_2 hydrogenation to higher alcohols, Applied Catalysis B: Environment and Energy, 345, 2024, 123691.

[10] Yang Wang, Kangzhou Wang, Baizhang Zhang, Xiaobo Peng, Xinhua Gao, Guohui Yang, Han Hu, Mingbo Wu, Noritatsu Tsubaki, Direct Conversion of CO_2 to Ethanol Boosted by Intimacy-

Sensitive Multifunctional Catalysts, ACS Catalysis, 11, 2021, 11742-11753.

[11] Di Xu, Mingyue Ding, Xinlin Hong, Guoliang Liu, Shik Chi Edman Tsang, Selective C_2^+ Alcohol Synthesis from Direct CO_2 Hydrogenation over a Cs-Promoted Cu-Fe-Zn Catalyst, ACS Catalysis, 10, 2020, 5250-5260.

[12] Qian Zhang, Sen Wang, Rui Geng, Pengfei Wang, Mei Dong, Jianguo Wang, Weibin Fan, Hydrogenation of CO_2 to higher alcohols on an efficient Cr-modified CuFe catalyst, Applied Catalysis B: Environment and Energy, 337, 2023, 123013.

[13] Baojian Chen, Caixia Zhu, Haozhe Feng, Teng Li, Zhihao Liu, Zhenzhou Zhang, Yingluo He, Noritatsu Tsubaki, Enhancing Higher Alcohols Selectivity in CO_2 Hydrogenation over FeCu Catalysts via Mg Modification, Catalysis Today, 463, 2026, 115614.

[14] Haiyan Yang, Zhangqian Wei, Jian Zhang, Yaru Dang, Shenggang Li, Xianni Bu, Zixuan Zhou, Chenfan Gong, Hao Wang, Jiong Li, Yang Liu, Yong Yang, Tianci Xiao, Chengyuan Liu, Yuhan Sun, Peng Gao, Tuning the selectivity of CO_2 hydrogenation to alcohols by crystal structure engineering, Chem, 10, 2024, 2245-2265.

[15] Wenhang Wang, Xiangyu Guo, Yang Wang, Simin Lin, Xinhua Gao, Jie Liang, Jinqiang Zhang, Jinghao Xie, Hu Jiang, Fengliang Cao, Yongjie Chen, Guohui Yang, Thomas Frauenheim, Mingqing Wang, Tao Xing, Yiwu Lu, Qiang Liu, Kostya S. Novoselov, Noritatsu Tsubaki, Mingbo Wu, Transformation of CO_2 to C_2^+ alcohols by tailoring the oxygen bonding via Fe-based tandem catalyst, Nature Communications, 16, 2025, 7265.

[16] Minghui Zhao, Xiaofan Hou, Mingming Peng, Lijiang Fan, Kenji Kamiya, Eika W. Qian, Effects of Glucose on Structure and Performance of KFeCuZr Catalyst for Higher Alcohols Synthesis from CO_2 Hydrogenation, ACS Sustainable Chemistry & Engineering, 14, 2026, 7275-7285.

[17] Zhongtao Sun, Jielang Huang, Kexin Feng, Zijie Ji, Dongyuan Liu, Chongchong Wu, Yi Zhang, Effects of initial iron oxide on forming C_2^+ alcohols via CO_2 hydrogenation, Chemical Engineering Journal, 537, 2026, 176413.

[18] Yuling Ma, Shuang Liu, Xin Han, Lei Ye, Haitao Xu, Lingtao Kong, Jiangbing Li, Xin Pu, Jichang Liu, Efficient Hydrogenation of CO_2 to Higher Alcohols over Cu-Zn-Fe Catalysts: The Role of $ZnFe_2O_4$ Spinel Precursor, ACS Sustainable Chemistry & Engineering, 2026, 14, 2026, 1467-1476.